



Article

An Anchoring Capacity Study Focused on a Wheel's Curvature Geometry for an Autonomous Underwater Vehicle with a Traveling Function during Contact with Loose Ground Containing Water

Akira Ofuchi ¹, Daisuke Fujiwara ² and Kojiro Iizuka ^{1,*}

¹ Functional Control Systems, Graduate School of Engineering and Science, Shibaura Institute of Technology, Saitama 337-0003, Japan; nb22108@shibaura-it.ac.jp

² Department of Mechanical & Electrical Engineering, Faculty of Engineering, Mechanical and Electrical Engineering, Suwa University of Science, Nagano 391-0213, Japan; fujiwara@rs.sus.ac.jp

* Correspondence: iizuka@shibaura-it.ac.jp

Abstract: The current scallop fishery sector allows many scallops to remain in specified fishing zones, and this process leads to heavy losses in the sector. Scallop fishermen aim to harvest the remaining scallops to reduce their losses. To achieve this, a fisherman must understand the scallop ecology on the seafloor. In our previous study, we proposed a method for measuring scallops using wheeled robots. However, a wheeled robot must be able to resist disturbance from the sea to achieve high measurement accuracy. Strong anchoring of wheels against the seafloor is necessary to resist disturbance. To better understand anchoring performance, we confirmed the wheel anchoring capacity in water-containing sand in an experiment. In this experiment, we towed fixed wheels on water-containing sand and measured the resistance force acting between the wheel and the sand. Afterward, we considered the resistance force as the wheel anchoring capacity on the water-containing sand. The experimental results capture the tendency for the anchoring capacity of sand with/without water to increase with sinkage. The results also demonstrate that the anchoring capacity of water-containing sand is lower than that of non-water-containing sand. However, the results indicate that when the wheels possess lugs, their presence tends to increase the wheels' anchoring capacity in water.

Keywords: scallop; underwater; wheel; anchoring capacity; soft ground; seabed



Citation: Ofuchi, A.; Fujiwara, D.; Iizuka, K. An Anchoring Capacity Study Focused on a Wheel's Curvature Geometry for an Autonomous Underwater Vehicle with a Traveling Function during Contact with Loose Ground Containing Water. *Geotechnics* **2024**, *4*, 350–361. <https://doi.org/10.3390/geotechnics4020019>

Received: 20 February 2024

Revised: 11 March 2024

Accepted: 15 March 2024

Published: 25 March 2024



Copyright: © 2024 by the authors. Licensee MDPI, Basel, Switzerland. This article is an open access article distributed under the terms and conditions of the Creative Commons Attribution (CC BY) license (<https://creativecommons.org/licenses/by/4.0/>).

1. Introduction

Current scallop fishing activities involve the release of scallops into a fishing zone and their harvest after they have grown to a specific size. The use of this method helps scallop fishermen to catch around 5.5 million tons of scallops annually. However, the figure of 5.5 million tons represents only 40–60% of the total released scallops. The remaining scallops represent a loss of approximately CNY 50 billion. Scallop fishermen aim to harvest the remaining scallops to increase their catches. The causes of scallop loss include predation by starfish and mortality due to rough seas. However, the other causes of loss are not yet fully understood. To understand these causes, it is necessary to investigate the relationship between the scallops' physical condition and the environment on the seafloor.

The authors of previous studies have attempted to understand scallops' physical condition by visualizing them on the seafloor. This method involves a camera being lowered from a ship and the ship being steered so that photographs of the seabed can be taken [1]. The seabed photographs that are taken will show the number and location of scallops over a wide area. Then, information from these photographs can be used to indicate the scallop distribution in the fishing zone. However, using their distribution alone prevents one from fully understanding scallops' physical condition. In light of this problem, fishermen require a new method to obtain more information other than simply the

scallops' location and number to understand their physical condition. One way to increase the amount of measurement information gained is to directly measure the detailed physical quantities of scallops (mass, size, and detailed shell condition). This method requires the examination of the seafloor to avoid causing stress to the scallops and reducing their value. Therefore, our research team proposes a method to measure the physical quantity of scallops directly on the seafloor using an underwater robot as shown in Figure 1. The steps of the proposed method are described below:

- First, lower the robot with a robotic arm and camera from the ship.
- Second, use the robot's camera to recognize scallops.
- Third, navigate the robot to the location of the scallop until the robot arm reaches the scallop.
- Fourth, instruct the robot to seize the scallop and measure its physical quantity.
- Fifth, instruct the robot to release the scallop and begin to recognize other scallops.

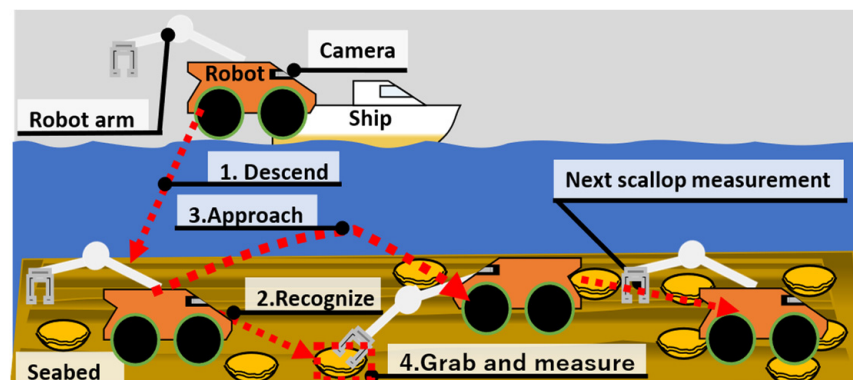


Figure 1. Scallop physical quantity measurement method involving the use of robots.

To perform the procedure above, the proposed robot requires a scallop recognition function, a scallop acquisition function, the ability to move near scallops, and a scallop measurement function. The authors of previous studies have examined the recognition of scallops on the seafloor through the use of cameras [2–6]. Additionally, the authors of previous studies have also examined the use of an underwater robotic arm [7–9] and a specific gripper mechanism for catching scallops [10,11]. Therefore, scallops could be recognized and acquired on the seafloor by adding robots to the methods used in previous studies. In addition, approaching scallops is possible with the use of existing underwater robots. Existing underwater robots can be broadly classified into floating and grounding types. The floating type swims underwater. An example of a floating-type underwater robot is a drone [12,13]. The floating type is affected to a lesser extent by terrain as it travels without contact with the ground. Thus, floating robots have high mobility performance and can easily approach scallops. In contrast, a grounding-type underwater robot moves over the seafloor. Examples of the grounding type are crawled, legged, and wheeled robots [14–22]. This type is easily affected by terrain when in contact with the seafloor. Therefore, the grounding type is inferior to the floating type in terms of mobility performance. However, the robot must maintain its posture to improve measurement accuracy. If the robot's posture is unstable, this results in decreased measurement accuracy. In addition, the robot must maintain its posture because an unstable posture can lead to errors in measurements. The floating type cannot achieve good performance and maintain its posture since this type of underwater robot is always floating and unable to maintain a fixed posture. Therefore, the grounding type is more suitable for the proposed method.

Among grounding robots, we focus on wheeled robots because of their simple structure and ease of control. However, there are concerns about wheeled robots with regard to maintaining their posture on the seabed. If a wheeled robot is placed on the seabed, ocean currents apply force to the robot and disturb the maintenance of the robot's position on the seabed. Robots must strongly anchor their wheels on the seafloor to resist ocean currents.

Thus, the robot’s wheel design needs to take into consideration mobility performance and good anchorage to the ground. To achieve such a design, research on the relationship between fixed wheels and water-containing soft ground surfaces is necessary. Although there are studies in the literature related to compression and shear force measurement tests on water-containing ground surfaces, there is a lack of research on the forces exerted by fixed wheels on this type of ground [23–25]. Therefore, in this study, we focused on the interaction between fixed wheels and the water-containing ground and carried out experiments to confirm the anchoring capacity of wheels acting on this type of ground to better understand this interaction.

2. Problems of Scallop Measurement with Wheeled Robots on the Seabed

When a wheeled robot is on the seafloor, the ocean current causes disturbance to the robot. This disturbance makes it possible for the robot to move in an unintended direction. This movement then causes errors in the measurements taken and reduces measurement accuracy. The robot’s wheels must possess strong anchoring capacity on the soft ground where scallops live in order to resist this disturbance. The robot’s wheel anchoring capacity on the soft ground is the combined force of the passive earth pressure F_1 (Equation (1)) and the shear resistance F_2 (Equation (2)), as shown in Figure 2 [26,27]. F_1 and F_2 occur when disturbance acts on the soil adjacent to a fixed wheel on the soft ground. When the external force pushes the fixed wheels on the soft ground, the wheels generate a triangular soil mass (Area A) on the wheels, as shown in Figure 2. The shear resistance generated between Area A and the soil below Area A is F_2 . F_1 is the combined passive earth pressure generated when Area A acts on Area B like a plate. Other forces are predicted to be small compared to F_1 and F_2 , and in this current study, we did not consider such forces.

$$F_1 = \gamma z_0^2 \tan^2\left(45^\circ + \frac{\varphi}{2}\right) \tag{1}$$

$$F_2 = \tau_{max} \left[1 - e^{-jk/kx}\right] = (c + \sigma \tan \varphi) \left[1 - e^{-jk/kx}\right] \tag{2}$$

where γ is the density of the ground, z_0 is the sinkage, φ is the internal friction angle, c is the adhesion force, σ is the vertical stress acting on the bottom of the soil mass under the wheel, jk is the shear displacement, and kx is the shear displacement coefficient.

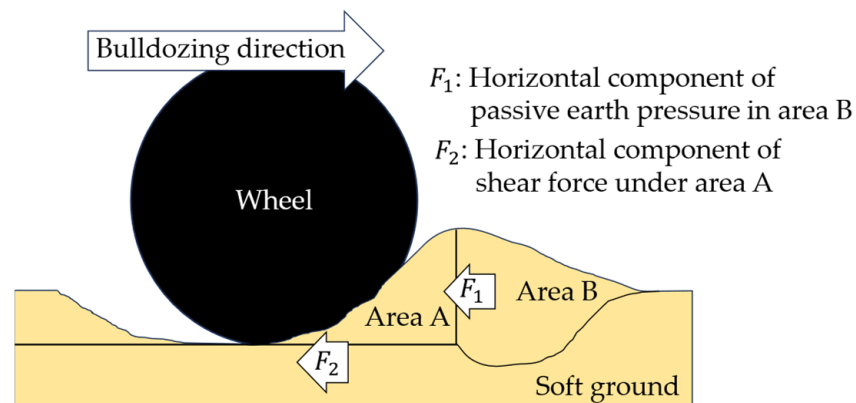


Figure 2. Stress in sand applied to wheels.

The vertical stress σ in Equation (2) is similarly affected by wheel width, wheel radius, and wheel sinkage because Equation (3) (the combined vertical component of the stress acting on the wheel from the ground W) depends on width, radius, and sinkage, as shown in Figure 3 [26].

$$W = BR \int_{-\theta_s}^{\theta_s} p(\theta) \cos \theta = BR \left(\frac{k_c}{B} + k_\varphi\right) R^n \times (\cos \theta - \cos \theta_s)^n \cos \theta \tag{3}$$

where $p(\theta)$ is the stress in the sand under the wheel, k_c is the coefficient governed by the adhesive force of the sand, k_ϕ is the coefficient governed by the internal friction angle in the sand, B is the wheel width, R is the wheel radius, n is the sinking index, θ is the wheel angle at an arbitrary point, and θ_s is the wheel angle at the starting point of the wheel and ground contact [28].

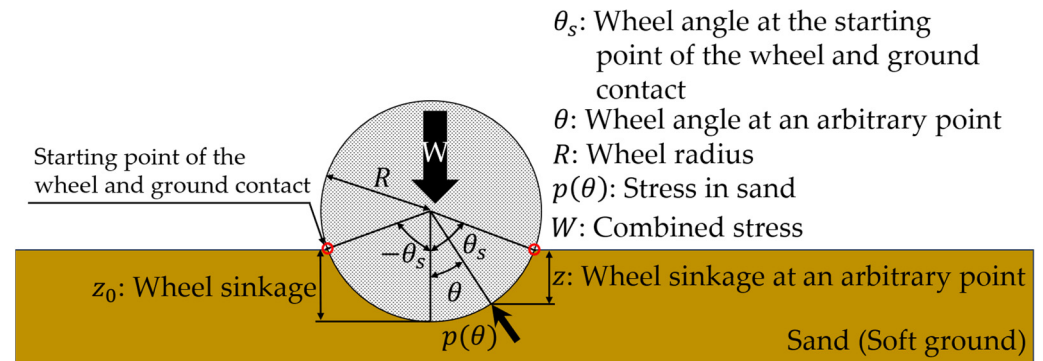


Figure 3. Relationship between sinkage and the wheel on loose soil.

Equation (1) suggests that the anchoring capacity increases with the increase in sinkage. Moreover, Equation (2) and Figure 2 suggest that increasing the radius slightly increases the anchoring capacity. Additionally, Equation (3) suggests that the right-hand side depends on the radius and width. Equation (3) shows that the required sinkage decreases when the width and radius increase.

The equations above can be used to determine the anchoring capacity on non-water-containing sand. However, these equations do not consider the effect of water on the sand. The authors of previous studies have found that the more water there is in the soft ground, the lower the shear resistance is [23–25]. This fact shows that the shear resistance F_2 applied to a wheel on water-containing soft ground, such as the seabed, is smaller. Thus, the anchorage force on the water-containing sand surface is expected to be lower than that on non-water-containing sand. However, the combined earth pressure F_1 in water is unclear because the soil mass of Area A and the soil mass of Area B have different conditions compared to the soil mass of the non-water-containing sand surface due to the influence of water. To clarify the anchoring capacity on water-containing sand, we need to understand how the pressure of Area B changes in water. Understanding this change is difficult because the properties of the soil become very complex as a result of the inclusion of water. Therefore, in this study, we conducted an experiment in which an external force is applied to a fixed wheel to generate F_1 and F_2 to investigate how F_1 and F_2 change depending on the presence of water and to confirm the anchoring performance of the wheel on water-containing sand.

Specifically, we first submerged the wheel in sand with water. In the next step, we towed the wheel laterally to simulate the lateral force applied by ocean currents. Afterward, the shear direction force generated at this time was measured. We conducted this experiment in the presence and absence of water to understand the specific effects of water.

3. Experiments to Confirm the Effect of Water on Wheel Anchoring Capacity

3.1. Experimental Procedure

Equations (1)–(3) show that the wheel anchorage force on soft ground increases with wheel sinkage, wheel width, and wheel radius. This fact suggests the possibility of obtaining high anchorage force even in water-containing sand by having wheels with a great degree of sinkage, a large wheel width, and a large wheel radius. However, the shear resistance of sand decreases with the increase in water content. Thus, the shear resistance of sand saturated with water is low. Additionally, low shear strength decreases the interlocking of the sand, and the ground particles are more likely to move, resulting in lower earth pressure. Low pressure can increase the difficulty of obtaining the anchoring force that can

resist disturbances such as ocean currents, even if the wheel has a high degree of sinkage, a large width, and a large radius. Therefore, we experimented with water-containing sand to confirm the effects of water on wheel anchorage force in this type of sand and the relationship between the wheel sinkage, wheel width, wheel radius, and wheel anchorage force in the sand.

The procedure in the experiment used to confirm the effect of water on the wheel anchorage capacity acting on the ground is shown in Figure 4. As shown in Figure 4a, the test apparatus consists of two wheels in contact with the ground, a force sensor to measure the forces acting on the ground and the wheels, a linear actuator to tow the wheels, and water-containing sand with a mixture of water and sand.

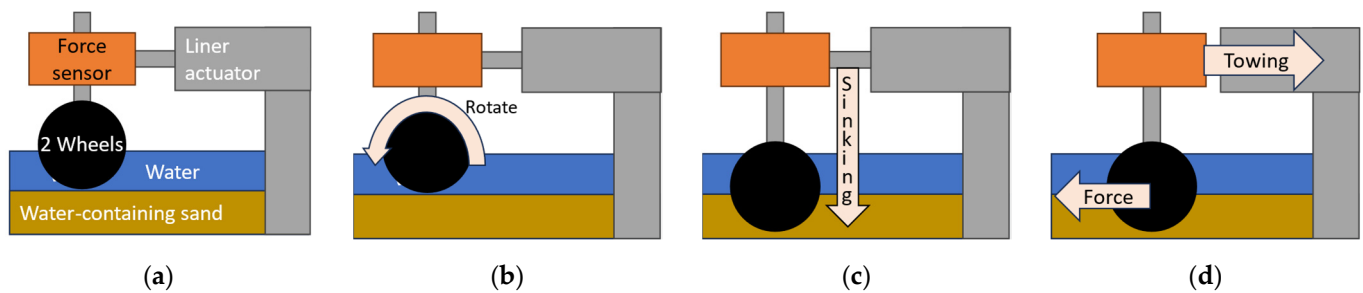


Figure 4. Experimental procedure for measuring the resistance force. (a) Initial state; (b) rotating state; (c) sinking state; (d) towing state.

The experimental procedure is performed as follows:

- First, carefully set the wheels on the water-containing sand (Figure 4a). The sinkage at this time must be set to 0 mm (static sinkage). When the wheels are on the soil, they sink into the soil due to their weight. This form of sinkage is defined as static sinkage.
- Second, rotate the wheels (number of rotations: 0, 0.5, 1, 1.5, or 2) to increase the degree of sinkage (Figure 4b,c).
- Third, measure the degree of sinkage. The measured sinkage degree is taken as the initial sinkage.
- Fourth, the linear actuator tows the wheel unit, and the force sensor measures the resistance force acting on the wheel (Figure 4d).

In the experiment, we used both the non-water-containing sand and water-containing sand to confirm the effect of water on the relationship between wheel anchorage force and the soft ground. Additionally, we used multiple experimental wheel conditions (sinkage, width, and radius) to confirm the relationship between the wheel conditions and the wheel anchorage force on water-containing sand.

Note that the water conditions (water pressure, water quality, and other conditions) used in the experiment vary greatly from those on the actual seafloor. This difference makes it difficult to completely clarify the wheel anchorage capacity on the seafloor. However, since this experiment focuses on confirming the relationship between wheel anchorage force and soft ground changes with water, we ignored the effects of water pressure, water quality, and other elements.

3.2. Experimental Conditions and Environment

The experimental machine (Figure 5) consists of two wheels, a force sensor, a linear actuator, and water-containing/non-water-containing sand placed in a plastic tank. Additionally, the wheel distance indicates the distance between both wheels. The wheels used in the experiment are all made of PLA. Their shapes are shown in Figure 6. Wheel A is the base wheel; wheel B has a smaller radius than wheel A; wheel C has the same radius and width as wheel A, albeit with the addition of lugs; and wheel D has a smaller wheel width than wheel A. Table 1 summarizes the specifications of the experimental machine.

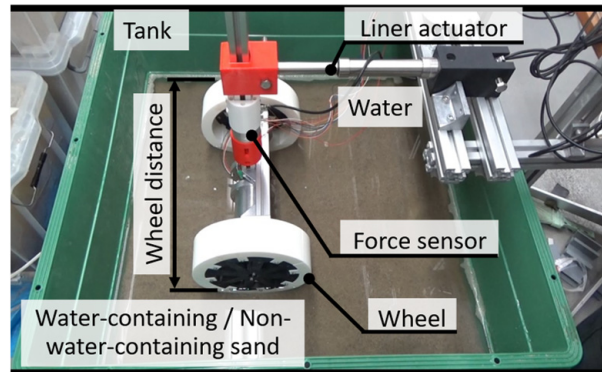


Figure 5. Experimental machine.

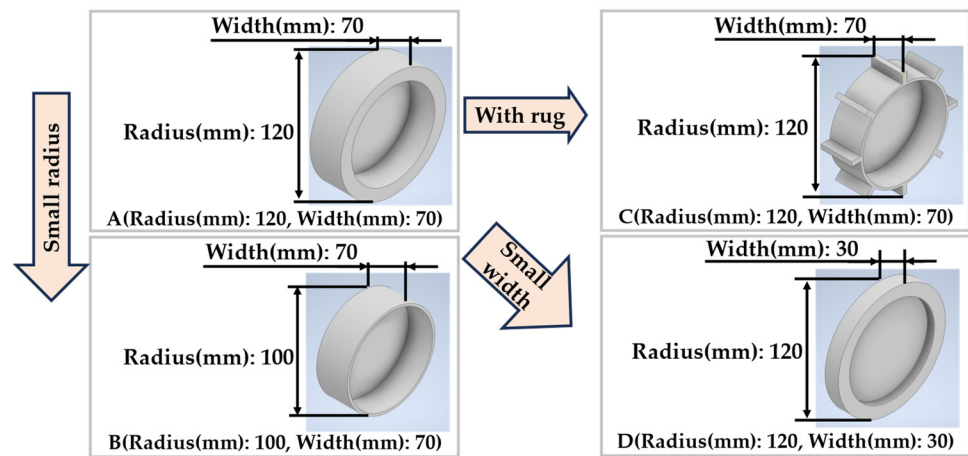


Figure 6. Difference in wheel shape.

Table 1. Specifications of the experimental device.

Name	Model	Role	
Liner actuator	Concens A/S Linear actuator con35(con350100–141220+449900)	Wheel towing	
Force sensor	PFS055YA251U6	Measuring anchoring capacity	
Name	Parameter	Numerical value	
Testing machine unit	Mass of testing machine (kg)	6.4	
	Wheel distance (mm)	450	
Tank	Width (mm)	847	
	Length (mm)	847	
	Height (mm)	341	
Water	Type	Freshwater	
	Depth (mm)	80	
Sand	Type	Silica sand No. 5	
	Depth (mm)	50	
Wheeled type	Radius (mm)	Width (mm)	Length of lug (mm)
A	120	70	0
B	100	70	0
C	120	70	20
D	120	30	0

3.3. Experimental Results and Considerations

Figure 7 shows images of the experimental procedure above (Figure 5). The experimental results are shown in Figures 8–10 and Table 2. Figure 8 shows the relationship

between the number of wheel rotations and the initial sinkage on each type of sand in Figure 7b. Figures 9 and 10 show the relationship between initial sinkage, towing time, and anchoring capacity when the wheel shown in Figure 7c is towed. Figures 9 and 10 show the anchoring capacity under different sand conditions. Table 2 summarizes the relationship between the number of rotations, the initial sinkage shown in Figure 8, and the maximum anchoring capacity shown in Figures 9 and 10. A description of the charts above and consideration of the experimental results are included below.

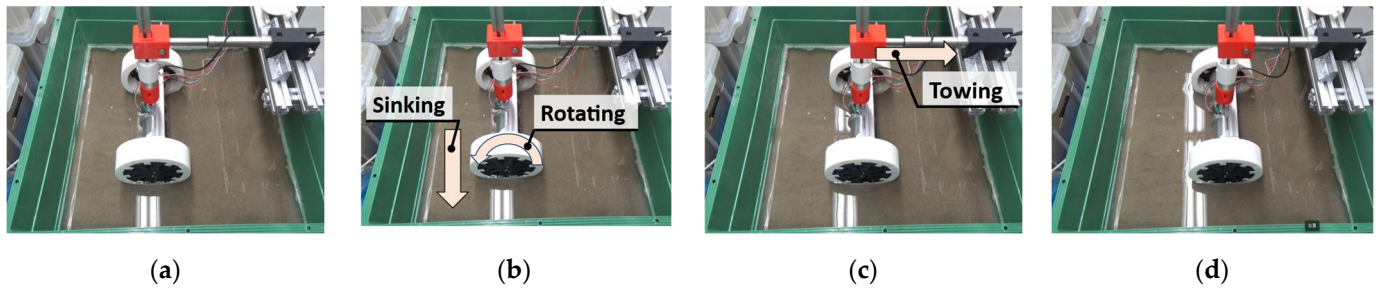


Figure 7. Images of the experiment: (a) initial state; (b) rotating and sinking states; (c) towing state; (d) end state.

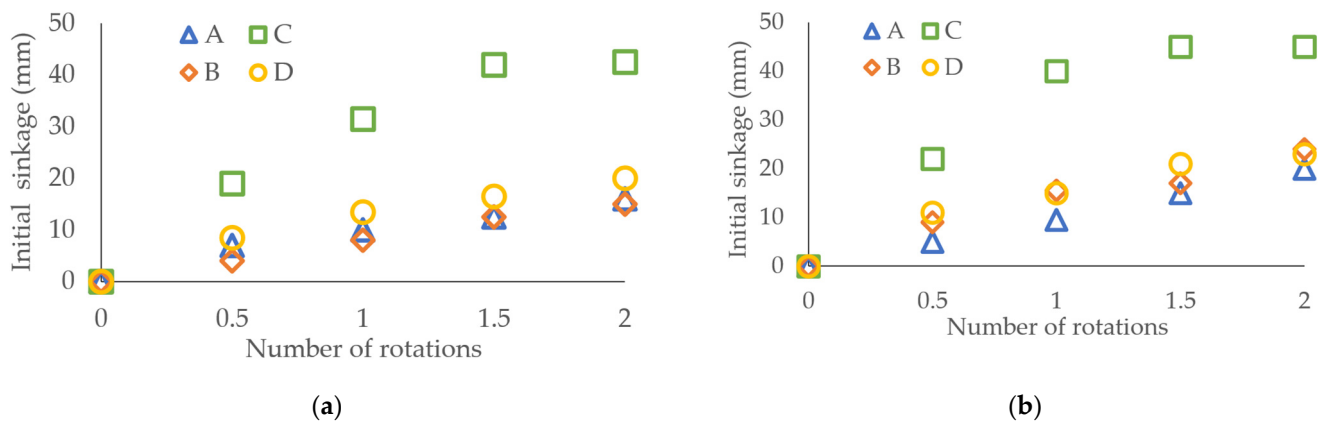


Figure 8. The relationship between the number of rotations and initial sinkage. The vertical axis represents the initial sinkage, and the horizontal axis represents the number of wheel spins. The legend shows the wheel shape. (a) Non-water-containing sand and (b) water-containing sand.

First, the relationship between the number of wheel rotations and the initial sinkage (Figure 8) shows a trend of increasing sinkage with more rotation on both types of sand. Additionally, as the wheel rotates on water-containing sand, the degree of sinkage is greater than on non-water-containing sand. In particular, wheel C, including lugs, is susceptible to sinkage as the lugs tend to concentrate stress. Wheels B and D, with a small radius and width, are susceptible to sinkage for the same reason.

Additionally, the relationship between initial sinkage and anchoring capacity (Figures 9 and 10) shows a trend of increasing anchoring capacity with greater initial sinkage on both types of sand. This trend corresponds to Equation (1) and indicates that increasing sinkage is also effective in water-containing conditions. The information displayed in Table 2 also indicates that the anchoring capacity on the water-containing sand tends to be lower than the anchoring capacity on the non-water-containing sand when comparing the maximum anchoring capacity of all wheels. For example, the decreasing trend can be seen in the fact that the anchoring capacity of wheel A (where the sinkage is 20 mm and the anchoring capacity is 27.5 N) on water-containing sand is smaller than that of wheel A (where the sinkage is 16 mm and the anchoring capacity is 36.6 N) on non-water-containing sand. This decreasing trend indicates that water exerts an effect of reducing the anchoring capacity on the soft ground.

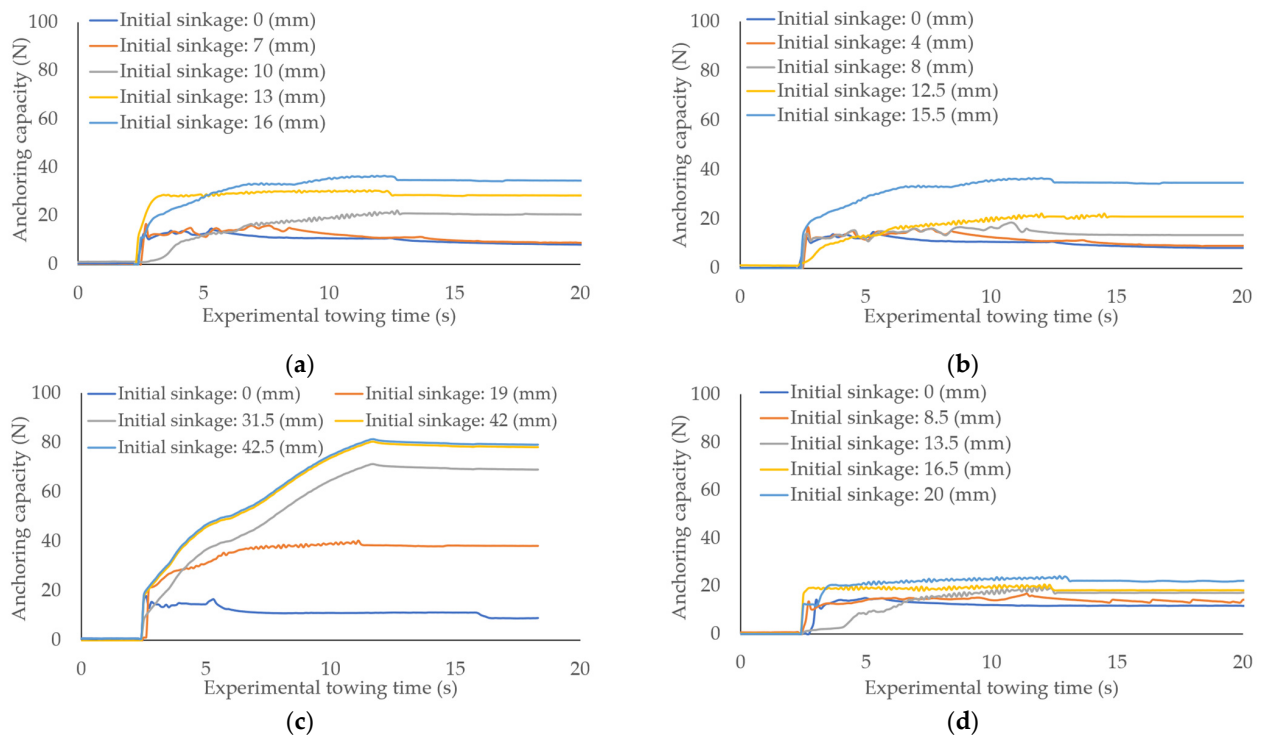


Figure 9. The relationship between the initial sinkage, experimental towing time, and anchoring capacity on non-water-containing sand. The horizontal axis represents the experimental towing time. The vertical axis represents the anchoring capacity. The legend shows the initial sinking amount. (a) Wheel A; (b) Wheel B; (c) Wheel C; (d) Wheel D.

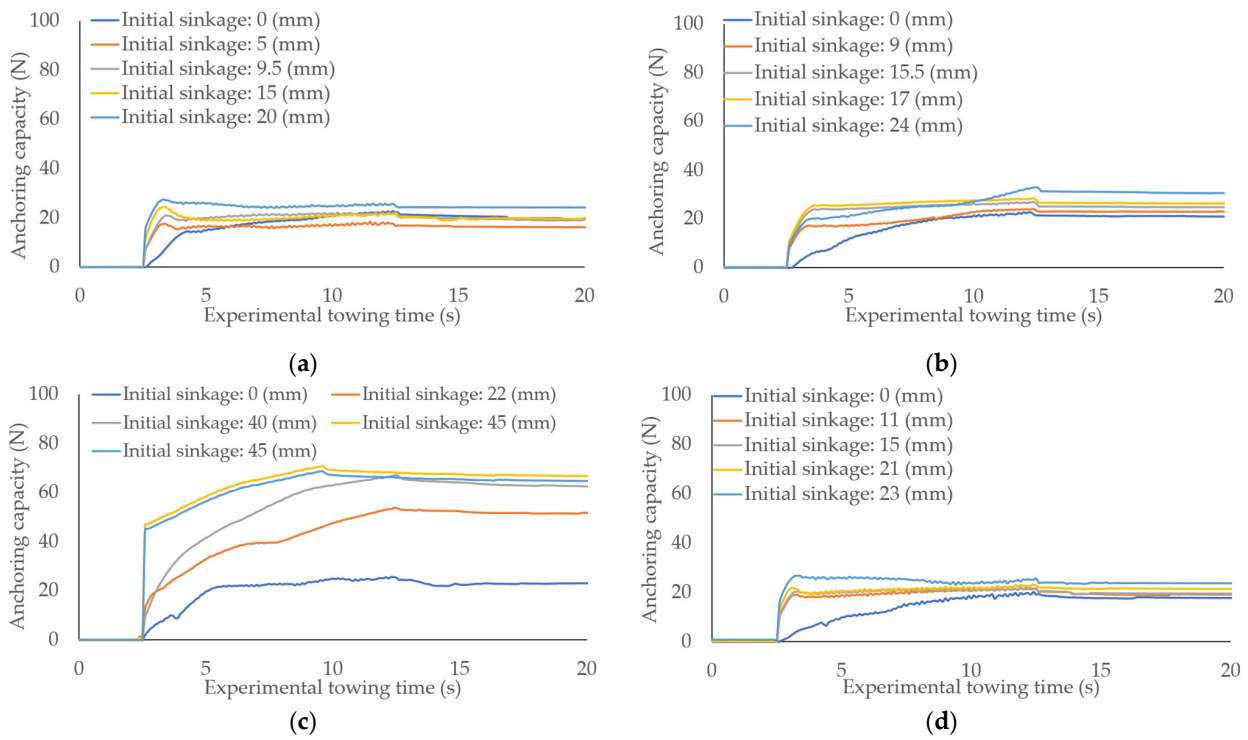


Figure 10. The relationship between the initial sinkage, experimental towing time, and anchoring capacity on water-containing sand. The horizontal axis represents the experimental towing time. The vertical axis represents the anchoring capacity. The legend shows the initial sinking amount. (a) Wheel A; (b) Wheel B; (c) Wheel C; (d) Wheel D.

Table 2. Relationship between the number of rotations, the initial sinkage, and the maximum anchoring capacity.

Wheel Type	Sand State	Number of Rotations	Initial Sinkage (mm)	Maximum Anchoring Capacity (N)
A (Base wheel)	Non-water-containing sand	0	0 (static sinkage)	14.7
		0.5	7	16.7
		1	10	22.2
		1.5	13	30.6
		2	16	36.6
	Water-containing sand	0	0	22.7
		0.5	5	18.4
		1	9.5	22.0
		1.5	15	24.4
		2	20	27.5
B (Small radius)	Non-water-containing sand	0	0 (static sinkage)	14.8
		0.5	4	16.9
		1	8	18.6
		1.5	12.5	22.2
		2	15.5	36.6
	Water-containing sand	0	0	22.7
		0.5	9	24.1
		1	15.5	26.9
		1.5	17	28.4
		2	24	32.9
C (With lugs)	Non-water-containing sand	0	0 (static sinkage)	17.8
		0.5	19	20.3
		1	31.5	71.3
		1.5	42	80.3
		2	42.5	81.3
	Water-containing sand	0	0	25.6
		0.5	22	53.7
		1	40	67.2
		1.5	45	70.7
		2	45	68.7
D (Small width)	Non-water-containing sand	0	0 (static sinkage)	15.0
		0.5	8.5	16.8
		1	13.5	19.8
		1.5	16.5	20.8
		2	20	24.2
	Water-containing sand	0	0	20.2
		0.5	11	21.7
		1	15	21.9
		1.5	21	23.2
		2	23	26.8

Note: When the wheel makes contact with the soil, the wheel sinks into the soil due to its weight. This form of sinkage is defined as static sinkage.

Additionally, Equation (2) and Figure 2 indicate that the larger the wheel width and radius for the same degree of sinkage, the higher the anchoring capacity. Equation (3) also suggests that the larger the width and radius, the higher the ground reaction force and the smaller the required sinkage. To confirm the increased trend in water, we compared the maximum anchoring capacity of each wheel when the sinkage was around the same as the value shown in Table 2. Table 2 shows that the anchoring capacity of wheel D (where the sinkage is 21 mm and the anchoring capacity is 23.2 N on water-containing sand) is smaller than that of wheel A (where the sinkage is 20 mm and the anchoring capacity is 27.5 N on water-containing sand). These results indicate that there is a tendency for an increase in anchoring capacity due to the increase in width, even in water. Therefore, the

increased trend from Equation (2) is consistent with the other results. Conversely, the results for the effect of radius are not consistent with the increased trend from Equation (2). Table 2 shows that the anchoring capacity of wheel B (where the sinkage is 15.5 mm and the anchoring capacity is 26.9 N on water-containing sand) is greater than that of wheel A (where the sinkage is 15 mm and the anchoring capacity is 24.4 N on water-containing sand). This result suggests that the smaller the radius, the greater the anchoring capacity in water. The possible reason for this result contradicting the trend in Equation (2) is that the wheel sinks during towing due to its buoyancy. Equation (2) and Figure 2 suggest that the anchoring capacity increases with the increase in radius when the degree of sinkage is identical. Equation (3) also suggests that the smaller the radius, the more likely the wheel is to sink. In fact, the results displayed in Figure 8b show that wheel B is more likely to sink than wheel A. Thus, wheel B, with its small radius, sinks more than wheel A while being towed. In light of the theory that the greater the degree of sinkage, the greater the anchoring capacity, the anchoring capacity of wheel B is expected to be greater than that of wheel A. In addition, the wheels are always buoyant in the water. Buoyancy decreases the downward force on the wheel, reducing the force required to support the wheel. This reduction lowers the rate of sinkage during towing. The greater the buoyancy, the stronger this reduction effect. Therefore, wheel A, which has a greater volume than wheel B, is subjected to greater buoyancy force and displays a stronger reduction effect. The combination of these effects led to a discrepancy between the experimental results and the trend in Equation (2). However, the reason for the agreement in increase by width and the disagreement in increase by radius is assumed that the trend of increase by radius is small in water. Furthermore, the anchoring capacity of wheel C (where the sinkage is 22 mm and the anchoring capacity is 53.7 N on water-containing sand) in water is greatest when the sinkage is close to 20 mm (Table 2). This is assumed to be due to the concentration of stress near the lugs. This concentration tightens the soil particles near the lugs and increases their anchoring capacity. The lugs also increase the amount of sand that is moved out from under the wheel, thus helping the wheel to sink (Figure 8). Therefore, the lugs can contribute to the greater anchoring capacity of the wheels.

The above results show that the anchoring capacity on water-containing sand is lower than the anchoring capacity on non-water-containing sand. The results also show that the wheel elements required to acquire high anchoring capacity in water are a high degree of sinkage, a large width, a small radius, and the presence of lugs. Under the same degree of sinkage, the effects of width and sinkage on anchoring capacity are consistent with the trends expressed in Equations (1) and (2). However, the effect of the radius, as explained in Equation (2), is possibly only small. In addition, these effects are not necessarily valid. Equation (3) shows that wheels with a larger width and radius are less likely to sink. This means that a larger wheel width and radius increase the number of revolutions required for the wheel to sink. This increase makes wheel sinkage inefficient. Moreover, increasing the width and the radius of the wheel increases its buoyancy due to the increased volume and makes sinking difficult. In addition, the use of lugs is suitable if they are appropriately sized. However, the use of lugs that are too large increases the risk of breakage. Excessively large lugs also result in too much sand being removed from under the wheels and prevent the robot from moving. Therefore, for a wheeled robot to maintain high posture performance and mobility efficiency, its wheels must possess the appropriate width, radius, and number of lugs.

4. Conclusions

Through this research, our research team proposes a new method for measuring the physical properties of scallops on the seafloor using a wheeled robot. When using a wheeled robot in the proposed method, it is important to consider the robot's anchoring capacity on water-containing sand. However, research on wheel anchoring capacity on water-containing sand is lacking. Due to this lack of research, the degree of anchoring capacity that can be achieved on the seafloor remains unclear. Thus, to expand our un-

derstanding of wheel anchoring capacity, we conducted experiments with towing wheels on water-containing sand. From the results of our towing experiments, we came to the following conclusions:

- The anchoring capacity of the same wheel at the same sinkage level tends to be lower on water-containing sand. This fact suggests that water weakens the ground strength, and the wheeled robot's ability to maintain its posture on water-containing sand decreases.
- An increase in the sinkage level is effective at increasing the anchoring capacity of the wheel even underwater. The greater the degree of initial sinkage, the greater the anchoring capacity, even on water-containing sand.
- The wheel shape affects the wheel's anchoring capacity in water. Wheeled robots require appropriate wheel shapes for high posture maintenance performance and mobility efficiency.

The results of our experiments show that water weakens the ground strength and reduces the anchoring capacity of wheels in water. The results also show that the relationship between the degree of sinkage, the wheel shape, and the wheel anchoring capacity does not change significantly in water. This finding suggests that the wheel can obtain a high anchoring capacity by adjusting its degree of sinkage and shape. To adjust these parameters, it is necessary to understand the sand properties (cohesion, shear strength, and so forth) that are changed in the presence of water. Therefore, we plan to construct an equation and model for the anchoring capacity in water by quantitatively observing how the sand properties change in the presence of water. In addition, the experimental conditions must more closely reflect the operating conditions of a wheeled robot on the seafloor to confirm the effectiveness of the robot in actual conditions. Therefore, we plan to create a site simulating the seabed (in consideration of water, water current, sand properties, sand gradient, etc.) and a testbed. We then plan to use them to conduct experiments.

Author Contributions: Conceptualization, A.O.; methodology, A.O., D.F. and K.I.; software, A.O.; validation, A.O.; formal analysis, A.O.; investigation, A.O.; resources, A.O.; data curation, A.O.; writing—original draft preparation, A.O.; writing—review and editing, D.F. and K.I.; visualization, A.O.; supervision, K.I.; project administration, K.I.; funding acquisition, K.I. All authors have read and agreed to the published version of the manuscript.

Funding: This research received no external funding.

Data Availability Statement: The datasets presented in this article are not readily available because the data are part of an ongoing study. Requests to access the datasets should be directed to email the corresponding author.

Conflicts of Interest: The author declares no conflicts of interest.

References

1. Enomoto, K.; Toda, M.; Kuwahara, Y. Detection Method of Scallop and Asteroid from Seabed Video. In Proceedings of the IAPR International Conference on Machine Vision Applications, Kyoto, Japan, 20–23 May 2013.
2. Enomoto, K.; Toda, M.; Kuwahara, Y. Extraction Method of Scallop Area in Gravel Seabed Images for Fishery Investigation. *Inst. Electron. Inf. Commun. Eng.* **2010**, *93*, 1754–1760. [[CrossRef](#)]
3. Enomoto, K.; Toda, M.; Kuwahara, Y. Extraction Method of Scallop Areas Using Shelly Rim Features Considering Bottom Sediment of Sand. In Proceedings of the IAPR Conference on Machine Vision Applications, Nara, Japan, 13–15 June 2011.
4. Enomoto, K.; Toda, M.; Shimizu, Y.; Kuwahara, Y. Fluorescent Staining for Detecting Larvae of Japanese Scallops *Mizuhopecten Yessoensis*. *Trans. Inst. Syst. Control Inf. Eng.* **2018**, *31*, 419–427.
5. Enomoto, K.; Toda, M.; Kuwahara, Y. Extraction Method of Scallop Area in Sand Seabed Images. *Inst. Electron. Inf. Commun. Eng.* **2014**, *97*, 130–138. [[CrossRef](#)]
6. Enomoto, K.; Toda, M.; Kuwahara, Y.; Masaki, W.; Hatanaka, K. Scallop Detection from Gravel-Seabed Images for Fishery Investigation. In Proceedings of the IAPR International Conference on Machine Vision Applications, Yokohama, Japan, 20–23 May 2009.
7. Pandian, R.S.; Sakagami, N. Extraction, System Integration Aspects of Underwater Vehicle-Manipulator Systems for Oceanic Exploration. *Meas. Control* **2008**, *47*, 830–836.

8. Weerakoon, T.; Sonoda, T.; Nassiraei, F.A.A.; Godler, I.; Ishii, K. Underwater Manipulator for Sampling Mission with AUV in Deep-Sea. In Proceedings of the JSME Conference on Robotics and Mechatronics, Fukuoka, Japan, 10–13 May 2017.
9. Zheng, X.; Tian, Q.; Zhang, Q. Development and Control of an Innovative Underwater Vehicle Manipulator System. *J. Mar. Sci. Eng.* **2023**, *11*, 548. [[CrossRef](#)]
10. Ofuchi, A.; Iizuka, K.; Fujiwara, D.; Enomoto, K.; Toda, M.; Kuwahara, Y.; Miyoshi, K. Proposal of gripper for scallop harvesting using underwater negative pressure. *J. Jpn. Soc. Des. Eng.* **2021**, *56*, 449–464. [[CrossRef](#)]
11. Ofuchi, A.; Iizuka, K.; Fujiwara, D. Study on the Applicability Considering on the Relationship between Shape and Flexibility of the Adsorption Gripper Tip. In Proceedings of the 2022 7th International Conference on Control and Robotics Engineering (ICCRE), Beijing, China, 15–17 April 2022.
12. Nagashima, Y.; Taguchi, N.; Ishimatsu, T. Development of a Compact Hybrid Underwater Vehicle Using Variable Vector Propeller. In Proceedings of the ISARC International Symposium on Automation and Robotics in Construction, Tokyo, Japan, 3–5 October 2006.
13. Itoh, R.; Okazaki, T. Development of an Underwater Robot for Detecting Shallow Water in a Port. *J. Robot. Mechatron.* **2020**, *34*, 64–71. [[CrossRef](#)]
14. Naruse, T. Development of Bottom-Reliant Type Underwater Robots. *J. Robot. Mechatron.* **2014**, *26*, 279–286. [[CrossRef](#)]
15. Xia, M.; Lu, H.; Yang, J.; Sun, P. Multi-Body Dynamics Modeling and Straight-Line Travel Simulation of a Four-Tracked Deep-Sea Mining Vehicle on Flat Ground. *J. Mar. Sci. Eng.* **2023**, *5*, 1005. [[CrossRef](#)]
16. Picardi, G.; Chellapurath, M.; Iacoponi, S.; Stefanni, S.; Laschi, C.; Calisti, M. Bioinspired underwater legged robot for seabed exploration with low environmental disturbance. *Sci. Robot.* **2020**, *11*, eaaz1012. [[CrossRef](#)] [[PubMed](#)]
17. Guan, H.; Luo, T.; Lian, W.; Lei, Y. Design of Adsorption Track Wheel for Underwater Wall-climbing Robot. In Proceedings of the 2022 6th International Conference on Robotics and Automation Sciences (ICRAS), Wuhan, China, 9–11 June 2022; IEEE: Piscataway, NJ, USA, 2022.
18. Picardi, G.; Astolfi, A.; Chatzievangelou, D.; Aguzzi, J.; Calisti, M. Underwater legged robotics: Review and perspectives. *Bioinspir. Biomim.* **2023**, *18*, 031001. [[CrossRef](#)] [[PubMed](#)]
19. Surveyor Amphibious Surface Inspection and Load Delivery Robot. Available online: https://www.newtonlabs.com/robot_surveyor.html (accessed on 18 January 2024).
20. Aquatic Rover Goes for a Drive under the Ice. Available online: <https://www.jpl.nasa.gov/news/aquatic-rover-goes-for-a-drive-under-the-ice> (accessed on 18 January 2024).
21. Boh, T.; Billingsley, J.; Bradbeer, R.S.; Hodson, P. Terramechanics based traction control of underwater wheeled robot. In Proceedings of the OCEANS'10, Sydney, Australia, 24–27 May 2010; IEEE: Piscataway, NJ, USA, 2010.
22. Ofuchi, A.; Iizuka, K.; Fujiwara, D. Fundamental Experiment on Mobility of Wheeled Underwater Mobile Robot on Water-containing Sand. In Proceedings of the JSME Conference on Robotics and Mechatronics, Nagoya, Japan, 22–25 May 2013.
23. Bouri, D.; Krim, A.; Brahim, A.; Arab, A. Shear strength of compacted Chlef sand: Effect of water content, fines content and others parameters. *Stud. Geotech. Mech.* **2020**, *42*, 18–35. [[CrossRef](#)]
24. Lanzerstorfer, C. The water content of sand required for the maximum strength for building sand castles. *Carpathian J. Earth Environ. Sci.* **2019**, *14*, 61–66. [[CrossRef](#)]
25. Khen, S.F.; Azam, S.; Raghunandan, M.E.; Clark, R. Compressive Strength of Compacted Clay-Sand Mixes. *Adv. Mater. Sci. Eng.* **2014**, *2014*, 921815. [[CrossRef](#)]
26. Fujiwara, D.; Oshima, T.; Iizuka, K. Measuring the Normal Stress Distribution Acting on a Locked-Wheel of Push–Pull Locomotion Rovers via a Wheel Sensor System. *Sensor* **2020**, *20*, 4434. [[CrossRef](#)] [[PubMed](#)]
27. Wong, J.Y. Mechanics of vehicle-terrain interaction/terrmechanics. In *Theory of Ground Vehicles*, 2nd ed.; Mech, E., Editor, B., II, Eds.; John Wiley & Sons: Hoboken, NJ, USA, 2007; Volume 3, pp. 100–146.
28. Beeker, M.G. Mechanics of Off-the-Road Locomotion. *Proc. Inst. Mech. Eng. Automob* **1962**, *16*, 22–44. [[CrossRef](#)]

Disclaimer/Publisher’s Note: The statements, opinions and data contained in all publications are solely those of the individual author(s) and contributor(s) and not of MDPI and/or the editor(s). MDPI and/or the editor(s) disclaim responsibility for any injury to people or property resulting from any ideas, methods, instructions or products referred to in the content.